PLEASE CITE THIS ARTICLE AS DOI: 10.1063/5.0191532

# Non-Toxic, Precious-Metal-Free Titanium-Based Metallic Glasses with Exceptional Glass-Forming **Ability and High Specific Strength**

Lei Chen, <sup>1,2</sup> Tittaya Thaiyanurak, <sup>1,2</sup> Zhengming Wang, <sup>1,2</sup> Madeline Ayers, <sup>3</sup> Natalia Zaitseva, <sup>4</sup> Donghua  $Xu^{1,2*}$ 

<sup>1</sup>Materials Science Program, Oregon State University, Corvallis, OR 97331, U.S.A.

<sup>2</sup>School of Mechanical, Industrial and Manufacturing Engineering, Oregon State University, Corvallis, OR 97331, U.S.A.

<sup>3</sup>School of Civil and Construction Engineering, Oregon State University, Corvallis, OR 97331, U.S.A.

<sup>4</sup>School of Electrical Engineering and Computer Science, Oregon State University, Corvallis, OR 97331, U.S.A.

\*Corresponding author. Mailing address: 2000 SW Monroe Ave., 204 Rogers Hall, Corvallis, OR 97331, U.S.A.; Email: Donghua.Xu@oregonstate.edu; Phone: (541)737-7027.

ORCID: 0000-0001-5018-5603.

PLEASE CITE THIS ARTICLE AS DOI: 10.1063/5.0191532

## Abstract

Titanium-based metallic glasses (TBMGs) are attracting broad interest due to their simultaneous light weight, superhigh strength and specific strength, exceptional wear- and corrosion-resistance and biocompatibility, desirable for electronic, biomedical, and aerospace applications. However, the glassforming ability (GFA) of TBMGs, except some containing significant amount of toxic (Be) or precious (Pd, Ag) elements, is disappointingly low, as manifested by a critical casting diameter (dc) no more than 6 mm, which significantly restricts their manufacturing and applications. Here we report our discovery of a series of TBMGs in the (TiZrHf)<sub>x</sub>(CuNi)<sub>y</sub>(SnSi)<sub>z</sub> pseudo-ternary system. These alloys possess an exceptionally large d<sub>c</sub>, reaching up to 12 mm, doubling the current record for Be and precious-metal free TBMGs. Moreover, these alloys exhibit a low density (7.0-7.3 g/cm<sup>3</sup>), high fracture-strength (up to ~2700 MPa), high specific fracture-strength (up to ~370 N m g<sup>-1</sup>), and even good plasticity with a plastic strain of up to 9.4% upon compression. They also possess high activation energy for crystallization and high atomic packing efficiency which provide an initial physical account for their exceptional GFA and manufacturability.

PLEASE CITE THIS ARTICLE AS DOI: 10.1063/5.0191532

Metallic glasses (MGs) are next-generation metals/alloys that possess an overall disordered atomic structure (with short-range ordering but no long-range translational or rotational symmetry). Because of the unique structure, MGs behave drastically different than crystalline metals/alloys (including high entropy alloys) when responding to external stimuli. Upon mechanical loading, they show much higher (by several hundred percent, typically) strength, hardness, elastic strain limit and wear resistance. Upon reheating, they undergo glass transition, softening and superplastic flow far below the melting temperature. Upon casting from the molten state, they acquire the pre-designed shape precisely, without suffering from crystallization shrinkage. These unique behaviors/properties make MGs promising candidates for a range of structural and functional applications (e.g., consumer electronics, sports utilities, precision thermoplastic molding, metalinsulator-metal thin film diodes, micro- and nano-electromechanical devices). 1-8 Among the many different types of MGs, Ti-based MGs (TBMGs) are particularly attractive because of their added advantages of light weight, high specific strength, exceptional corrosion resistance, and biocompatibility. TBMGs possess great potential to be used in biomedical devices (including human body implants) and aerospace components. Therefore, a great deal of effort has been devoted to discovering and developing TBMG alloys.9-20

Nevertheless, current TBMGs are plagued by their poor glass-forming ability (GFA). Most TBMGs must be manufactured with at least one dimension (the shortest one) kept below 6 mm in order to obtain a fully glassy structure. 10,11,16-20 This threshold in the shortest dimension is termed as the critical casting diameter (for a cylinder) or thickness (for a plate), dc. Exceeding the dc will result in partial or complete crystallization (due to insufficient cooling rate). Many other types of MG alloys (e.g., Zr-based, 21 Fe-base, 22 Cu-based,  $^{23,24}$  Hf-based  $^{25}$ ) have been discovered with d<sub>c</sub> exceeding 10 mm. For TBMGs, in contrast, only certain alloys in the Ti-Zr-Cu-Fe(Ni)-Be12 and Ti-Zr-Cu-Pd-Sn13,14 systems have been found to reach above the 10 mm landmark. Unfortunately, these alloys contain substantial amounts of the toxic element Be or the precious metal Pd. Other than the Be or Pd bearing alloys, a dc of 7 mm has been reported for an alloy in the Ti-Zr-Cu-Fe-Ag-Sn-Si system which still relies on the precious metal Ag. 15

PLEASE CITE THIS ARTICLE AS DOI: 10.1063/5.0191532

Here, we report our discovery of a series of Be and precious-metal free TBMGs in the (TiZrHf)<sub>x</sub>(CuNi)<sub>y</sub>(SnSi)<sub>z</sub> pseudo-ternary system. We show that alloys with compositions around  $(TiZrHf)_{55}(CuNi)_{40.5}(SnSi)_{4.5}$ , more specifically,  $Ti_{55-a-b}Zr_aHf_bCu_{40.5-c}Ni_cSn_{3.2}Si_{1.3}$  (3<a<4.5, 6<b<10 and 4<c<15), have exceptional GFA and manufacturability. In particular, the Ti<sub>42.1</sub>Zr<sub>4.3</sub>Hf<sub>8.6</sub>Cu<sub>28.3</sub>Ni<sub>12.2</sub>Sn<sub>3.2</sub>Si<sub>1.3</sub> alloy exhibits a d<sub>c</sub> of 12 mm, the largest for all Be and precious-metal free TBMGs known to date. We also report the thermal and mechanical properties of these alloys and examine the physical origin of their exceptional GFA and manufacturability through crystallization activation energy and atomic packing efficiency.

Alloy ingots of different compositions were prepared through arc-melting mixtures of ultrasonically cleansed Ti (99.9+%, crystal bar), Zr (99.9+%, crystal bar), Hf (99.2+%, crystal bar), Cu (99.99%, oxygen-free shot), Ni (99.98%, slugs), Sn (99%, shot), and Si (99.9+% lump) pieces. Prior to the melting of the raw materials, the arc melter chamber was vacuumed to ~3×10-4 mbar residual pressure and filled with ultrahigh purity (UHP) argon, and then a Zr-getter was used (melted) to absorb the remaining oxygen and further clean the atmosphere. The alloy ingots were flipped and re-melted at least eight times each to acquire complete chemical homogeneity. Then, the ingots were melted again and tilt cast into a copper mold placed underneath the melting stage to form cylindrical rods of various diameters. Crosssections of the cast rods were analyzed with an X-ray diffractometer (Rigaku Smartlab) using a Cu- $K_{\alpha}$ source to reveal the amorphous or crystalline structure. Thermal behaviors, including glass transition and crystallization, of the alloys were studied with a differential scanning calorimeter (DSC, Mettler Toledo DSC3) at a heating rate of 0.333 K/s in a flowing nitrogen atmosphere. For the best composition  $(Ti_{42.1}Zr_{4.3}Hf_{8.6}Cu_{28.3}Ni_{12.2}Sn_{3.2}Si_{1.3})$ , DSC scans at additional heating rates (0.083, 0.167, 0.333, 0.500, 0.667, and 0.833 K/s) were conducted to obtain the crystallization activation energy based on the Kissinger method. Compression tests were performed on specimens of ~1.35 mm diameter and 2.7 mm length using the Deben MT5000 (maximum load: 5 kN) test module at a nominal strain rate of ~6×10<sup>-4</sup> s<sup>-1</sup>. Vickers hardness was measured on a LECO M400A microhardness tester using a pyramid-shaped indenter, a 500

PLEASE CITE THIS ARTICLE AS DOI: 10.1063/5.0191532

AIP Publishing gf load and a 15 s dwelling time. Densities were determined according to the Archimedes' Principle using the Pioneer Scale – OHAUS PA84 and Density measurement kit.

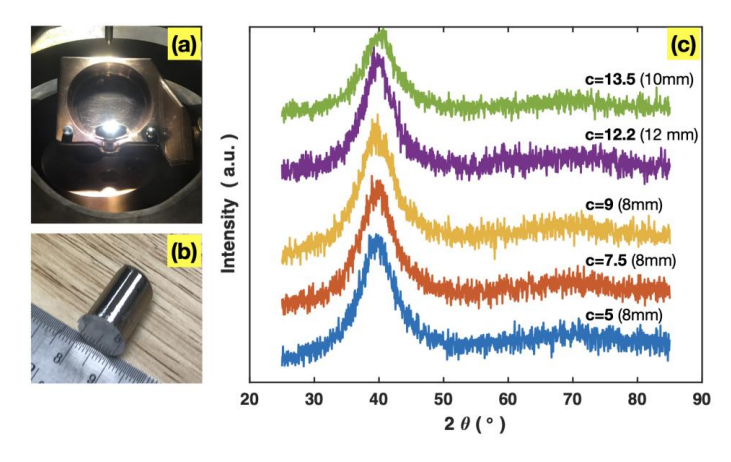


Fig. 1. (a) tilt casting setup inside the arc melter; (b) an exemplary 12 mm diameter cast rod; (c) X-ray diffraction patterns of Ti<sub>42,1</sub>Zr<sub>4,3</sub>Hf<sub>8,6</sub>Cu<sub>40,5-c</sub>Ni<sub>c</sub>Sn<sub>3,2</sub>Si<sub>1,3</sub> with varied Ni content and cast diameter.

Figure 1(a) shows the tilt casting setup inside the arc melter, with an alloy ingot sitting on the melting stage and a copper mold placed under. Figure 1(b) is the photo of a 12 mm diameter cast rod of the Ti<sub>42.1</sub>Zr<sub>4.3</sub>Hf<sub>8.6</sub>Cu<sub>28.3</sub>Ni<sub>12.2</sub>Sn<sub>3.2</sub>Si<sub>1.3</sub>, as an example. The cast surface is very smooth and reflective, typical of metallic glass samples. Figure 1(c) presents the X-ray diffraction (XRD) patterns of the cast rods of Ti<sub>42.1</sub>Zr<sub>4.3</sub>Hf<sub>8.6</sub>Cu<sub>40.5-c</sub>Ni<sub>c</sub>Sn<sub>3.2</sub>Si<sub>1.3</sub> alloys with varied Ni content (c=5, 7.5, 9, 12.2, 13.5) and diameters (8, 10 and 12 mm). These patterns only exhibit diffuse maxima, without any sharp Bragg peaks. This ascertains the fully amorphous nature of the cast rods. In the previous research on TBMGs, fully amorphous structure at these diameters was obtained only for alloys containing substantial amounts of the toxic Be or the precious metal Pd. <sup>10-14</sup> The Ti<sub>42.1</sub>Zr<sub>4.3</sub>Hf<sub>8.6</sub>Cu<sub>28.3</sub>Ni<sub>12.2</sub>Sn<sub>3.2</sub>Si<sub>1.3</sub> alloy discovered here, with a d<sub>c</sub> of 12 mm, stands out as the non-toxic and precious-metal free TBMG with the highest GFA and manufacturability as of today. One previous study reported a d<sub>c</sub> of 6 mm for Ti<sub>41.5</sub>Zr<sub>2.5</sub>Hf<sub>5</sub>Cu<sub>37.5</sub>Ni<sub>7.5</sub>Si<sub>1</sub>Sn<sub>5</sub>, <sup>16</sup> which is in the same alloy system as in the present work but different zone of the compositional space. Our alloys here employ

PLEASE CITE THIS ARTICLE AS DOI: 10.1063/5.0191532

a higher content of Ti+Zr+Hf, and lower contents of Cu+Ni and Sn. The striking improvement in the dc achieved here highlights the importance of finding the right compositions in the effort of developing highly processable and manufacturable MGs.

Table 1. Critical casting diameter  $d_{\circ}$ , density  $\rho$ , Vickers hardness  $H_{v}$ , yield strength  $\sigma_{v}$ , fracture strength  $\sigma_f$ , specific fracture strength  $\sigma_{f,S}$ , plastic strain (at fracture)  $\varepsilon_p$ , glass transition temperature  $T_g$  and onset crystallization temperature  $T_x$ , of the TBMGs discovered in this work.

Alloy composition	dc	ρ	$H_{ m v}$	$\sigma_y$	$\sigma_f$	$\sigma_{f,s}$	$\varepsilon_p$	$T_{\mathrm{g}}$	$T_{\rm x}$
(in at.%)	(mm)	(g	$(kg/mm^2)$	(GPa)	(GPa)	(N m/g)	(%)	(K)	(K)
		$/cm^3)$							
$Ti_{42.1}Zr_{4.3}Hf_{8.6}Cu_{35.5}Ni_5Sn_{3.2}Si_{1.3}$	8	7.3	594	1.94	2.6	356	3.9	675	726
$Ti_{42.1}Zr_{4.3}Hf_{8.6}Cu_{33}Ni_{7.5}Sn_{3.2}Si_{1.3}$	≥8	7.3	606	1.98	2.4	329	2.8	679	730
$Ti_{42.1}Zr_{4.3}Hf_{8.6}Cu_{31.5}Ni_{9}Sn_{3.2}Si_{1.3}$	≥8	7.3	609	1.99	2.7	370	6.1	680	729
$Ti_{42.1}Zr_{4.3}Hf_{8.6}Cu_{28.3}Ni_{12.2}Sn_{3.2}Si_{1.3}\\$	12	7.3	611	2.00	2.6	356	3.1	691	736
$Ti_{42.1}Zr_{4.3}Hf_{8.6}Cu_{27}Ni_{13.5}Sn_{3.2}Si_{1.3}$	10	7.3	615	2.01				692	735
$Ti_{45.1}Zr_{3.3}Hf_{6.6}Cu_{33}Ni_{7.5}Sn_{3.2}Si_{1.3}$	8	7.0	595	1.94	2.5	357	9.4	677	728

The densities ( $\rho$ , listed in Table 1) of the  $Ti_{42.1}Zr_{4.3}Hf_{8.6}Cu_{40.5\text{-c}}Ni_cSn_{3.2}Si_{1.3}$  (c=5, 7.5, 9, 12.2, 13.5) alloys are all measured to be 7.3 g/cm<sup>3</sup>, insensitive to the partition between the Cu and the Ni contents (due to the similarity of the two elements in their densities). This is close to the 7.0 g/cm3 of  $Ti_{41.5}Zr_{2.5}Hf_5Cu_{37.5}Ni_{7.5}Si_1Sn_5$  and 6.85 g/cm $^3$  of the Pd-bearing  $Ti_{40}Zr_{10}Cu_{34}Pd_{14}Sn_2$  TBMGs reported in the literature. 11 It is noted that the Hf content has a strong impact on the alloy density here (due to the high density of Hf). At a lower Hf content, the Ti<sub>45.1</sub>Zr<sub>3.3</sub>Hf<sub>6.6</sub>Cu<sub>33</sub>Ni<sub>7.5</sub>Sn<sub>3.2</sub>Si<sub>1.3</sub> alloy reaches a density of 7.0 g/cm<sup>3</sup>, while still retaining an excellent GFA with d<sub>c</sub> equal to 8 mm.

Also listed in Table 1 are the Vickers hardness  $(H_v)$  values of the present TBMGs, which fall in the range from ~590 to 620 kg/mm<sup>2</sup>. The hardness displays an increasing trend as more Cu is substituted with Ni (all other elemental contents fixed). This is attributable to the stronger interaction of Ni than Cu with the other five elements, as indicated by the more negative heat of mixing ( $\Delta H_{mix}$ ): -35, -49, -42, -4 and -40

This is the author's peer reviewed, accepted manuscript. However, the online version of record will be different from this version once it has been copyedited and typeset PLEASE CITE THIS ARTICLE AS DOI: 10.1063/5.0191532

kJ/mol for Ni with Ti, Zr, Hf, Sn, and Si, respectively, as opposed to the -9, -23, -17, 7, -19 for Cu. <sup>26</sup> For a similar reason (Zr and Hf interact more strongly than Ti with other elements), when some of the Zr and Hf percentages are shifted onto Ti while fixing all the other elements, the hardness decreases. The yield strength  $(\sigma_y)$  estimated from the relationship<sup>27</sup> (for isotropic materials)  $\sigma_y = \frac{H_y}{3}$  is also listed in Table 1, which is in reasonable agreement with the compression tests (at 2% elastic strain).

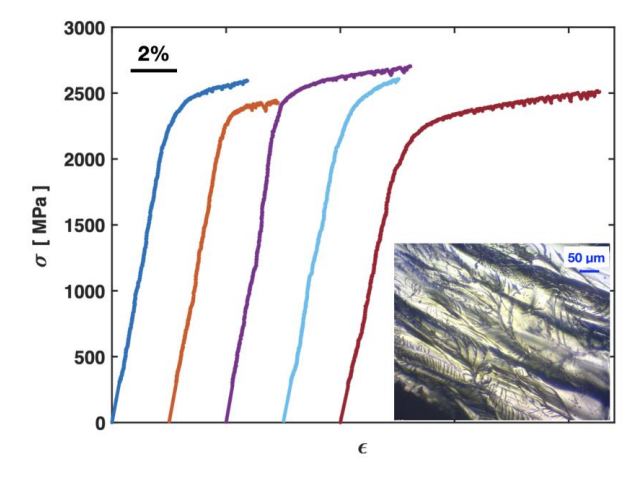


Fig. 2. Main panel: compressive stress-strain behaviors of, from left to right,

 $Ti_{42.1}Zr_{4.3}Hf_{8.6}Cu_{35.5}Ni_{5}Sn_{3.2}Si_{1.3},\ Ti_{42.1}Zr_{4.3}Hf_{8.6}Cu_{33}Ni_{7.5}Sn_{3.2}Si_{1.3},\ Ti_{42.1}Zr_{4.3}Hf_{8.6}Cu_{31.5}Ni_{9}Sn_{3.2}Si_{1.3},$   $Ti_{42.1}Zr_{4.3}Hf_{8.6}Cu_{28.3}Ni_{12.2}Sn_{3.2}Si_{1.3},\ Ti_{45.1}Zr_{3.3}Hf_{6.6}Cu_{33}Ni_{7.5}Sn_{3.2}Si_{1.3}.\ Inset:\ optical\ micrograph\ of\ fracture$   $surface\ of\ Ti_{45.1}Zr_{3.3}Hf_{6.6}Cu_{33}Ni_{7.5}Sn_{3.2}Si_{1.3}.$ 

Figure 2 (main panel) shows the engineering stress-strain curves for five of the present TBMGs obtained through compression tests. They all exhibit work hardening and serrated flow after yielding and several percent plastic strain ( $\varepsilon_p$ ) before fracture, alluding to the intrinsic plasticity in these glassy alloys. Particularly, the Ti<sub>45.1</sub>Zr<sub>3.3</sub>Hf<sub>6.6</sub>Cu<sub>33</sub>Ni<sub>7.5</sub>Sn<sub>3.2</sub>Si<sub>1.3</sub> alloy underwent a 9.4% plastic strain before fracture, which clearly surpasses most of the previously reported TBMGs (including the Be- and Pd-bearing ones). The fracture surface (inset in Fig. 2) exhibits significant vein-like features and a non-flat terrain with

PLEASE CITE THIS ARTICLE AS DOI: 10.1063/5.0191532

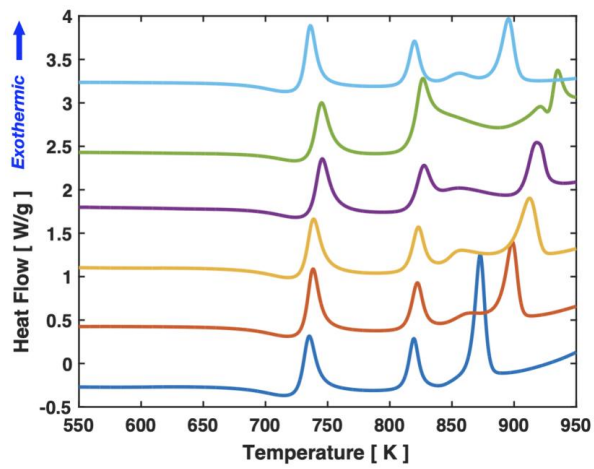


Fig. 3. Constant heating rate (0.333 K/s) DSC scans of, from bottom to top,  $Ti_{42.1}Zr_{4.3}Hf_{8.6}Cu_{35.5}Ni_5Sn_{3.2}Si_{1.3}$ ,  $Ti_{42.1}Zr_{4.3}Hf_{8.6}Cu_{33}Ni_{7.5}Sn_{3.2}Si_{1.3}$ ,  $Ti_{42.1}Zr_{4.3}Hf_{8.6}Cu_{27}Ni_{13.5}Sn_{3.2}Si_{1.3}$  and  $Ti_{45.1}Zr_{3.3}Hf_{6.6}Cu_{33}Ni_{7.5}Sn_{3.2}Si_{1.3}$ .

The curves were shifted vertically for clarity.

The glass transition and crystallization behaviors of the TBMGs, as measured by DSC at a heating rate of 0.333 K/s, are shown in Fig.3. They all show a clear glass transition, indicated by a downslope (endothermic) of the heat flow curve between 650 and 700 K, and multiple crystallization events signified by the up-pointing (exothermic) peaks above 720 K. The values of the glass transition temperature  $T_{\rm g}$  and

This is the author's peer reviewed, accepted manuscript. However, the online version of record will be different from this version once it has been copyedited and typeset PLEASE CITE THIS ARTICLE AS DOI: 10.1063/5.0191532

the onset crystallization (first event) temperature  $T_x$ , as determined by the commonly used two-tangent method, are listed in Table 1. The width of supercooled liquid region  $\Delta T = T_x - T_g$  falls in the range of 43 K to 51 K. As the composition is varied, the  $T_g$  exhibits a similar trend to the hardness discussed above, reflecting its fundamental dependence on the chemical interaction (bond strength) among the constituent elements.

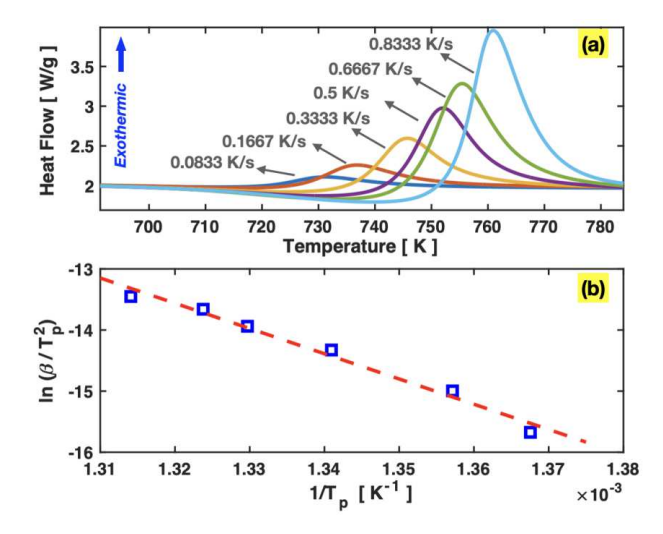


Fig. 4. (a) DSC scans of Ti<sub>42,1</sub>Zr<sub>4,3</sub>Hf<sub>8,6</sub>Cu<sub>28,3</sub>Ni<sub>12,2</sub>Sn<sub>3,2</sub>Si<sub>1,3</sub> with six different heating rates, showing the shift of the first crystallization peak; (b) Symbols: the Kissinger plot using the heating rate and peak temperature data from (a); dashed line: linear fit of the data.

The Kissinger method is often used to obtain the activation energy of a thermally activated process, such as a chemical reaction or phase transformation. It involves analyzing the correlation between the peak temperature of the process on a DSC scan and the heating rate used. Figure 4(a) shows the first (primary) crystallization event recorded by DSC at six different heating rates (from 0.0833 K/s to 0.8333 K/s) for  $Ti_{42.1}Zr_{4.3}Hf_{8.6}Cu_{28.3}Ni_{12.2}Sn_{3.2}Si_{1.3}$  which has a d<sub>c</sub> of 12 mm. A higher heating rate ( $\beta$ ) leads to an increase in the peak temperature ( $T_p$ ) as expected. According to the Kissinger method, the relationship

PLEASE CITE THIS ARTICLE AS DOI: 10.1063/5.0191532

between  $\beta$  and  $T_p$  can be reduced to:  $\ln\left(\frac{\beta}{T_p^2}\right) = -\frac{E_a}{R}\frac{1}{T_p} + constant$ , that is, a linear correlation between  $\ln\left(\frac{\beta}{T_p^2}\right)$  and  $\frac{1}{T_p}$ , with the slope equal to  $-\frac{E_a}{R}$  (where  $E_a$  is the activation energy, and R is the ideal gas constant). Figure 4(b) presents the experimental data (symbols) for  $\ln \left(\frac{\beta}{T_n^2}\right)$  and  $\frac{1}{T_n}$  and the linear fit (dashed line). The data follow the Kissinger model quite closely, as suggested by a high fitting-goodness R<sup>2</sup>=0.98. From the fitted slope, the activation energy  $E_a$  is determined to be 343 kJ/mol. This value is significantly higher than those reported in the literature for the first (primary) crystallization event in other TBMGs, for example, 287.6 kJ/mol for  $Ti_{40}Zr_{10}Cu_{36}Pd_{14}$ , 30 179 kJ/mol for  $Ti_{41}Zr_{25}Be_{28}Fe_6$ , 31 and 188 kJ/mol for  $Ti_{40}Zr_{10}Cu_{36}Pd_{14}$ , 30 179 kJ/mol for  $Ti_{41}Zr_{25}Be_{28}Fe_6$ , 31 and 188 kJ/mol for  $Ti_{40}Zr_{10}Cu_{36}Pd_{14}$ , 30 179 kJ/mol for  $Ti_{41}Zr_{25}Be_{28}Fe_6$ , 31 and 188 kJ/mol for  $Ti_{40}Zr_{10}Cu_{36}Pd_{14}$ , 30 179 kJ/mol for  $Ti_{40}Zr_{10}Cu_{36}Pd_{14}$ (Ti<sub>41</sub>Zr<sub>25</sub>Be<sub>28</sub>Fe<sub>6</sub>)<sub>93</sub>Cu<sub>7</sub>. <sup>31</sup> Since glass formation requires the avoidance of crystallization, the high value of  $E_a$  for crystallization obtained here partially explains the exceptional GFA of the present TBMG.

Another perspective to understand the origin of GFA of a MG is the atomic packing efficiency. It is known that MGs with good GFA often possess high atomic packing efficiency (APE). Efficient (dense) atomic packing can increase the viscosity of a supercooled liquid and decrease the atomic mobility and thereby suppress crystallization kinetically. The APE of a MG can be calculated  $^{23,25}$  as APE = $\rho \times \left(N_A \sum_i c_i \frac{4\pi}{3} r_i^3\right) / (\sum_i c_i m_i)$ , where  $\rho$  is the density of the alloy,  $N_A$  is the Avogadro's number, and  $c_i$ ,  $r_i$  and  $m_i$  are the atomic percent, atomic radius and atomic (molar) mass of the *i*th element, respectively. The APE hence calculated (using the atomic radii in Ref. 32) is equal to 0.763, 0.765, 0.766, 0.768, 0.769 for  $Ti_{42,1}Zr_{4,3}Hf_{8,6}Cu_{40.5-c}Ni_cSn_{3,2}Si_{1,3}$  (c=5, 7.5, 9, 12.2, 13.5), respectively, and 0.757 for Ti<sub>45.1</sub>Zr<sub>3.3</sub>Hf<sub>6.6</sub>Cu<sub>33</sub>Ni<sub>7.5</sub>Sn<sub>3.2</sub>Si<sub>1.3</sub>. These values are all greater than the well-known 0.74 for the close-packed fcc (face-centered-cubic) crystal structure. This reflects the efficient atomic packing in these TBMGs and aligns well with their exceptional GFA.

In summary, we have discovered a group of non-toxic and precious-metal free TBMGs that possess exceptional glass-forming ability. They belong to the pseudo-ternary (TiZrHf)-(CuNi)-(SnSi) system and possess chemical compositions around  $Ti_{55\text{-}a\text{-}b}Zr_aHf_bCu_{40,5\text{-}c}Ni_cSn_{3.2}Si_{1.3}$  (3<a<4.5, 6<b<10 and 4<c<15, This is the author's peer reviewed, accepted manuscript. However, the online version of record will be different from this version once it has been copyedited and typeset. PLEASE CITE THIS ARTICLE AS DOI: 10.1063/5.0191532

at.%). Fully glassy rods with diameters of 8 to 12 mm can be readily manufactured through tilt casting. Particularly, the  $Ti_{42.1}Zr_{4.3}Hf_{8.6}Cu_{28.3}Ni_{12.2}Sn_{3.2}Si_{1.3}$  alloy, with a critical casting diameter of 12 mm, presents the highest glass-forming ability and manufacturability for all non-toxic and precious-metal free TBMGs known to date. Moreover, the TBMGs here exhibit high fracture-strength (up to ~2700 MPa), high specific fracture-strength (up to ~370 N m g<sup>-1</sup>), and good plasticity with a plastic strain of up to 9.4% upon compression. High activation energy for crystallization and high atomic packing efficiency provide an initial account for the physical origin of their exceptional glass-forming ability, while a thorough understanding requires further investigation through detailed experimental and computational studies of kinetics, thermodynamics, and structural characteristics. The alloys discovered in this work are expected to accelerate the research and development and engineering applications of TBMGs as advanced structural and functional materials.

# Acknowledgement

This research was partially supported by the U.S. National Science Foundation under Grant No. DMR 2221854.

# **Data Availability Statement**

The data that support the findings of this study are available from the corresponding author upon reasonable request.

# PLEASE CITE THIS ARTICLE AS DOI: 10.1063/5.0191532

This is the author's peer reviewed, accepted manuscript. However, the online version of record will be different from this version once it has been copyedited and typeset.

## References

- <sup>1</sup> B. Sarac and J. Eckert, Progress in Materials Science **127**, 100941 (2022).
- <sup>2</sup> J. Schroers, Physics Today **66**, 32 (2013).
- J. Schroers, Advanced Materials 22, 1566 (2010).
- <sup>4</sup> J. F. Loffler, Intermetallics **11**, 529 (2003).
- <sup>5</sup> W. L. Johnson, Mrs Bulletin **24**, 42 (1999).
- <sup>6</sup> A. L. Greer, Science **267**, 1947 (1995).
- E. W. Cowell, N. Alimardani, C. C. Knutson, J. F. Conley, D. A. Keszler, B. J. Gibbons, and J. F. Wager, Advanced Materials 23, 74 (2011).
- <sup>8</sup> G. Kumar, H. X. Tang, and J. Schroers, Nature **457**, 868 (2009).
- <sup>9</sup> P. S. Chen, P. H. Tsai, T. H. Li, J. S. C. Jang, J. C. C. Huang, C. H. Lin, C. T. Pan, and H. K. Lin, Materials 16, 5935 (2023).
- <sup>10</sup> M. Zhang, Y. Song, H. Lin, Z. Li, and W. Li, Frontiers in Materials 8, 814629 (2022).
- <sup>11</sup> P. Gong, L. Deng, J. S. Jin, S. B. Wang, X. Y. Wang, and K. F. Yao, Metals **6**, 264 (2016).
- L. Zhang, M. Q. Tang, Z. W. Zhu, H. M. Fu, H. W. Zhang, A. M. Wang, H. Li, H. F. Zhang, and Z. Q. Hu, Journal of Alloys and Compounds 638, 349 (2015).
- <sup>13</sup> S. L. Zhu, X. M. Wang, and A. Inoue, Intermetallics **16**, 1031 (2008).
- <sup>14</sup> H. Wang, E. S. Park, J. J. Oak, A. D. Setyawan, S. L. Zhu, T. Wada, X. M. Wang, A. Takeuchi, and H. Kato, Journal of Non-Crystalline Solids 379, 155 (2013).
- S. J. Pang, Y. Liu, H. F. Li, L. L. Sun, Y. Li, and T. Zhang, Journal of Alloys and Compounds 625, 323 (2015).
- <sup>16</sup> Y. J. Huang, J. Shen, J. F. Sun, and X. B. Yu, Journal of Alloys and Compounds **427**, 171 (2007).
- O. Gross, L. Ruschel, A. Kuball, B. Bochtler, B. Adam, and R. Busch, Journal of Physics-Condensed Matter 32, 264003 (2020).
- <sup>18</sup> Y. Liu, S. J. Pang, H. F. Li, Q. Hu, B. Chen, and T. Zhang, Intermetallics **72**, 36 (2016).
- <sup>19</sup> H. E. Khalifa and K. S. Vecchio, Journal of Non-Crystalline Solids **357**, 3393 (2011).

PLEASE CITE THIS ARTICLE AS DOI: 10.1063/5.0191532

- <sup>20</sup> C. Ma, H. Soejima, S. Ishihara, K. Amiya, N. Nishiyama, and A. Inoue, Materials Transactions 45, 3223 (2004).
- <sup>21</sup> A. Peker and W. L. Johnson, Applied Physics Letters **63**, 2342 (1993).
- <sup>22</sup> V. Ponnambalam, S. J. Poon, and G. J. Shiflet, Journal of Materials Research 19, 1320 (2004).
- <sup>23</sup> J. S. Saini, C. Palian, F. Q. Lei, A. Dyall, N. AuYeung, R. McQuade, S. K. Gupta, D. P. Cann, and D. H. Xu, Applied Physics Letters 116, 011901 (2020).
- <sup>24</sup> D. H. Xu, G. Duan, and W. L. Johnson, Physical Review Letters **92**, 245504 (2004).
- <sup>25</sup> J. S. Saini, J. P. Miska, F. Q. Lei, N. AuYeung, and D. H. Xu, Journal of Alloys and Compounds 882, 160896 (2021).
- <sup>26</sup> F. R. d. Boer, W. C. M. Mattens, R. Boom, A. R. Miedema, and A. K. Niessen, *Cohesion in metals* (North-Holland, Netherlands, 1988).
- <sup>27</sup> L. A. Davis, in *Mechanical Behavior of Rapidly Solidified Materials*, edited by S. M. L. Sastry and B. A. Macdonald (The Metallurgical Society, Inc., Warrendale, PA, 1986).
- <sup>28</sup> R. L. Blaine and H. E. Kissinger, Thermochimica Acta **540**, 1 (2012).
- <sup>29</sup> N. Mitrovic, S. Roth, and J. Eckert, Applied Physics Letters **78**, 2145 (2001).
- <sup>30</sup> T. Czeppe, A. Sypien, and A. Wierzbicka-Miernik, Journal of Materials Engineering and Performance **25,** 5289 (2016).
- <sup>31</sup> P. Gong, K. F. Yao, and S. F. Zhao, Journal of Thermal Analysis and Calorimetry **121**, 697 (2015).
- <sup>32</sup> D. B. Miracle, W. S. Sanders, and O. N. Senkov, Philosophical Magazine **83**, 2409 (2003)